

The dipper light curve of V715 Per: is there dust in the magnetosphere?

E. Nagel¹ and J. Bouvier²

¹ Departamento de Astronomía, Universidad de Guanajuato, Callejón de Jalisco S/N, Guanajuato, Gto, 36240, México
e-mail: e.nagel@ugto.mx

² Univ. Grenoble Alpes, CNRS, IPAG, 38000 Grenoble, France
e-mail: jerome.bouvier@obs.ujf-grenoble.fr

Received, 2020; accepted

ABSTRACT

Context. The dipper optical light curves in young stellar objects are commonly interpreted as partial or total occultation of the stellar radiation by dust surrounding the star.

Aims. In this work, we analyze the amplitude of the optical light curve of V715 Per, located in the young star forming region IC 348. Observations gathered over the years suggest that the light curve can be explained by dust extinction events.

Methods. In our model, the dust is distributed inside the magnetosphere according to the strength of the stellar magnetic field. The dust distribution is modulated by the vertical component of the field, whose axis is misaligned with respect to the rotational axis. We include a model for the evaporation of the dust reaching the magnetosphere in order to consistently calculate its distribution.

Results. For V715 Per, there is dust in the optically thick warp at the disk truncation radius. We suggest that the optical light curve is explained by extinction caused by dust reaching inside the magnetosphere. The dust distribution is optically thin and due to the high temperature and low density, it cannot survive for a long time. However because the grains rapidly move towards the stellar surface and the sublimation is not instantaneous, there is a layer of dust covering the magnetosphere responsible for the extinction.

Conclusions. Dust surviving the harsh conditions of the magnetospheric accretion flow may be responsible for some of the dipper light curves.

Key words. Accretion, accretion disks – circumstellar matter

Use \titlerunning to supply a shorter title and/or \authorrunning to supply a shorter list of authors.

1. Introduction

The study of optical and near-infrared light curves of young stellar objects (YSOs) provides information about the dust distribution around the object. Observed light curves of YSOs clearly show its variability (Alencar et al. 2010; Cody et al. 2014; Morales-Calderón et al. 2011; Stauffer et al. 2015, 2016), the different features allow to define different classes, suggesting the rich and complex dynamics occurring in the dusty disk. For the modeling of light curves showing periodicity of a few days, it is required to take into account the interaction of the magnetic field lines defining the stellar magnetosphere with the inner edge of the disk, in particular for dipper light curves. The magneto-hydrodynamical simulations by Romanova et al. (2013) show the formation of magnetospheric streams and a bending wave in the innermost disk regions. These time-dependent structures with variable height can be used to interpret the light curves.

For a YSO, the optical flux mainly comes from the star, thus, its variability either comes from changes of the spot distribution at the stellar surface or results from the extinction of the stellar light by circumstellar dust. We are analyzing the second mechanism here, such that we can directly extract the characteristics of the azimuthal dust distribution from the shape of the light curve. If the structures blocking the stellar radiation are optically thick, the color calculated between two optical wavelengths is constant in terms of phase. An object which has shown this kind of behavior in the past is AA Tau whose light curve can be interpreted with a non-axisymmetric optically thick warp in the innermost regions of the disk surrounding the star (Bouvier et al. 1999). They suggest that the warp is formed at the base of the magnetospheric streams caused by an inclined stellar magnetic field interacting with the disk. This idea was followed by others: Fonseca et al. (2014) studied V354 Mon, McGinnis et al. (2015) applied this for a large sample in NGC 2264, and Nagel & Bouvier (2019) studied the objects Mon-660, Mon-811, Mon-1140 and Mon-1308. The optical light curves analyzed in these works come from the CoRoT Space Telescope. Simultaneous observations with the Spitzer Space Telescope in the infrared allows to connect the behavior in both wavelength ranges, interpreted via the dust distributed around the star (McGinnis et al. 2015; Nagel & Bouvier 2019).

The YSO V715 Per is one of several objects that present light curves showing color changes consistent with circumstellar extinction (Barsunova et al. 2013, 2015, 2016). This behaviour is common in young UX Ori stars, one of the main characteristics of this type is stochastic brightness variations caused by extinction where the dust is located in the circumstellar environment. Grinin et al. (2018) analyze V715 Per in the vein of their previous works, where for 5 objects coming from a large set of T Tauri stars, the light curves can be explained by extinction (Barsunova et al. 2013, 2015, 2016). Also Sicilia-Aguilar et al. (2020) show that the quasi-periodic eclipses in the young dipper RX J1604.3-2130A can be explained with extinction at the base of the magnetospheric streams.

The stellar parameters of V715 Per are listed in Table 1. The first value for the stellar mass (M_{\star}) comes from Kirk & Myers (2011) and the one in parenthesis comes from LeBlanc et al.

Table 1. Parameters for V715 Per

$M_{\star}(M_{\odot})$	$R_{\star}(R_{\odot})$	$T_{\star}(K)$	$\dot{M}(M_{\odot}yr^{-1})$
0.906(0.56)	2.31	4205	5×10^{-9}

(2011). The values are different because LeBlanc et al. (2011) use the pre-main-sequence evolutionary models calculated by D’Antona & Mazzitelli (1997) while Kirk & Myers (2011) use the evolutionary tracks by Baraffe et al. (1998). The difference also depends on the way the bolometric luminosity L_{bol} is calculated because besides the spectral type, LeBlanc et al. (2011)’s value uses the J-band magnitude and Kirk & Myers (2011)’s value uses the estimated age of the object (1Myr). The stellar radius (R_{\star}) is from LeBlanc et al. (2011) and the stellar effective temperature (T_{\star}) is taken from Luhman et al. (2003) using the associated spectral type (K6) shown in Herbig (1998). The mass accretion rate (\dot{M}) is taken from Dahm (2008) where we take the mean of the values associated to the estimates using the *HeI*, *H α* and *CaII* lines. We remove the estimate using the R-band veiling because as mentioned in Dodin et al. (2012), if the veiling by lines is included, the depth changes varies for different photospheric lines such that the estimate of \dot{M} is not reliable in this case. Ruiz-Rodriguez et al. (2018) observed the system with ALMA but the result was a non-detection, preventing them from deriving an inclination for the system.

The aim of this paper is to present a model to explain the amplitude and period of the optical light curve of V715 Per showed in Grinin et al. (2018). In our model, the variation of the magnitude comes from phase-dependent extinction due to material located in the magnetospheric streams.

In Section 2 we describe the characteristics of the optical light curve of V715 Per, in Section 3 we show the relevant aspects of the modeling, in Section 4 we address two important questions, namely whether there is dust in the disk and whether there is dust in the magnetosphere. The free and fixed parameters of the model are described in Section 5 and in Section 6, the model is applied to V715 Per. Finally in Section 7 we present the conclusions of this study.

2. The characteristics of the periodic light curve of V715 Per

Grinin et al. (2018) present observations for the stellar system V715 Per in the optical (VRI bands) and in the infrared (JHK bands). They present photometric data compiled from different campaigns between 2003 and 2017. For this large time scale, they confirm the presence of low-amplitude periodic brightness variations $\Delta mag \sim 0.1$ with a period equal to 5.25days. Flaherty et al. (2013) photometrically studied this system with the Spitzer Space Telescope at 3.6 and 4.5 μ m over 40 days and detected a signal with a period of 14.7days, which is not the stellar rotation period. The keplerian radius corresponding to 5.25days is 0.0574AU. The bending wave formed by the hydrodynamical interaction of the stellar magnetic dipolar field and the gaseous disk (Romanova et al. 2013) is used for the physical interpretation of the data presented in Grinin et al. (2018). Because of the larger period, the IR light curve cannot be analyzed with the model used here, thus it is required another mechanism to explain the photometric Spitzer data (Flaherty et al. 2013) for this system. The aim of this work is explain the amplitude of the optical light curve. The interpretation

of its details requires full 3D-MHD simulations which take into account each scenario in a highly dynamical region. This endeavor is well beyond the goal of this work.

In Grinin et al. (2018), the observed period in the light curve of $P = 5.25$ days is interpreted by occultations of material located at the keplerian radius consistent with P . At this location, they assume that the material accreting radially in the disk is halted by the magnetic pressure associated with the stellar magnetic field (hereafter referred to as B). In other words, this radius also corresponds to the magnetospheric radius (R_{mag}) such that the occulting material belongs to the base of the magnetospheric streams, near the plane of the disk that transport material towards the stellar surface at the magnetic poles, where two hot spots are formed.

3. The model used to interpret the observations

3.1. The system geometry and physical mechanisms

The 5.25 day period is the one we are trying to interpret. A model consistent with this period involves material close to the star. The dust responsible to produce the stellar eclipses accretes in the disk reaching the outskirts of the magnetosphere located at the radius R_{mag} . The existence of dust inside the magnetosphere requires that the sublimation radius (R_{sub}) is smaller than R_{mag} . The disk regions close to the midplane are optically thick to the stellar radiation, thus, they are responsible to produce total or partial stellar eclipses. For the well-known system AA-Tau, the photometric data shaping the periodical optical light curve do not show color changes (Bouvier et al. 1999), thus, the dust responsible for it should be optically thick, which is in accord to an optically thick disk. For V715 Per the periodic brightness variations show color changes consistent with circumstellar extinction, thus this material should be located in an optically thin environment. For the model presented here, this region corresponds to the dust located in the magnetospheric streams. Note that the radial dust distribution is not important for this estimate because the matter is added along the line of sight (from now on los).

We use the model for the accretion along a non-inclined dipolar B presented in Hartmann et al. (1994) where the density is given by

$$\rho_H(R, \theta) = \frac{\dot{M}R_{\star} \times R^{-5/2} \times (4 - 3\text{sen}^2\theta)^{1/2}}{4\pi\left(\frac{R_{\star}}{R_{in}} - \frac{R_{\star}}{R_{out}}\right)(2GM_{\star})^{1/2} \times (1 - \text{sen}^2\theta)^{1/2}}. \quad (1)$$

Here, G is the gravitational constant, R is the spherical radius, θ is the poloidal angle, R_{in} and R_{out} corresponds to the inner and outer intersections of the magnetospheric stream with the disk plane. We fix these values as $R_{in} = 0.9R_{mag}$ and $R_{out} = R_{mag}$, as an order of magnitude estimate motivated by the simulations presented in Figure 8 in Romanova et al. (2013). When it is used in the code, we take into account that the dipole is inclined with respect to the rotational axis. As in

Hartmann et al. (1994), the material velocity corresponds to ballistic infall from rest following the B lines. Finally, the gas density inside the magnetosphere (ρ_{mag}) is given by

$$\rho_{mag}(R, \theta, \phi) = \rho_H(R, \theta) * \gamma * \frac{B_{pol}(\theta, \phi)}{B_{dip}}, \quad (2)$$

where ϕ is the azimuthal angle, B_{pol} is the poloidal magnetic field and B at R_\star is given by B_{dip} . This factor is included in order to modulate the density such that the gas is concentrated where the magnetic pressure is larger. The value for the free-dimensional parameter γ is such that ρ_{mag} is consistent with \dot{M} . Because the magnetic axis is inclined with respect to the rotational axis, B_{pol} depends on ϕ and θ . All this together, the gas distribution depends on the azimuthal (ϕ) and poloidal angles (θ) such that the optical depth varies for different los. The presence and amount of dust is estimated using the temperature calculated as an equilibrium between the heating of stellar radiation and cooling as a blackbody at such temperature. Two facts guarantee the presence of dust in the magnetosphere: 1) the grains do not sublimate instantaneously and 2) the free-fall time (t_{ff}) is just a few hours. This means that the dust can survive in a layer with an outer radius given by R_{mag} , its inner boundary depends on the timescale of sublimation (t_{sub}) and t_{ff} . In our modeling, the amount of dust in this layer is responsible to explain the deepness of the light curve at the various phases, as described in Section 6.

3.2. Details of the code used

According to a dust distribution around the star, the code calculates the total or partial extinction of the stellar radiation heading to the observer. For our particular aim, the dust is located inside the magnetosphere, which is limited by R_{mag} . The dust reservoir is the protoplanetary disk where the grains are slowly moving towards the star. At R_{mag} , the material find a radial equilibrium because the magnetic pressure is equal to the ram pressure, such that the vertical direction is the only available path to follow. As we are assuming that the gas ionization is enough for the particles to be frozen to the B -lines, then the gas and the dust attached will follow the path given by the B -lines almost perpendicularly to the midplane of the disk. The material leaving the disk form the magnetospheric streams which consist of B -lines that shrinks as B is increased when it approaches the stellar surface. This behavior is taken into account to calculate the expression for ρ_{mag} (see equation 2).

We assume that B is given by a dipolar magnetic field which is tilted with respect to the rotational axis by an angle β_{dip} (Gregory et al. 2010) with B at R_\star given by B_{dip} . In order to find B_{dip} , we use eq. 1 in Konigl (1991) substituting the values for R_{mag} , M_\star and \dot{M} . For the model presented here, $\beta_{dip} = 5deg$ and $B_{dip} = 398G$. Along with β_{dip} and B_{dip} , the longitude where the magnetic axis is tilted (ψ_{dip}) is the other free parameter that defines the stellar B . Because the star is azimuthally rotating, every section of the stellar surface crosses the los once every rotating period, which according to the modeling is equal to P . This means that the value ψ_{dip} is only relevant to

locate the magnetic structure with respect to the light curve phases without changing the shape of the latter.

4. Presence of dust

4.1. Is there dust in the disk at R_{mag} ?

For the stellar radiation that do not show color changes as in AA-Tau (Bouvier et al. 1999), the occulting structure should be optically thick. For the stellar system modeled here, this corresponds to the optically thick disk that is perturbed in the vertical direction to form the required structures according to each case. In this section, we answer the question, is there optically thick dust at R_{mag} for the stellar system V715 Per?

We use the stellar and disk parameters associated to this object (Grinin et al. 2018) which are shown in Table 1 to calculate the disk surface density

$$\Sigma = \frac{\dot{M}}{3\pi\alpha} \frac{\Omega\mu m_H}{KT_c} [1 - \sqrt{R_*/R}] \quad (3)$$

given by Lynden-Bell & Pringle (1974) for a viscous stationary disk. The viscosity is parameterized with α (we assume $\alpha = 0.01$ as typical), Ω is the keplerian angular velocity, μ is the molecular number, m_H is the hydrogen mass, K is the Boltzmann constant, T_c is the temperature at the midplane and R is the distance towards the star.

Using Σ , we calculate the disk density at R_{mag} with

$$\rho_{disk} = \frac{\Sigma}{2H}, \quad (4)$$

where $H = c_s/\Omega$ is the hydrostatic scale height and $c_s = \sqrt{\frac{KT_c}{\mu m_H}}$ is the sound speed. This results in

$$\rho_{disk}(R = R_{mag}) = 7.59 * 10^{-9} \times \left(\frac{\dot{M}}{5 \times 10^{-9} M_{\odot} \text{yr}^{-1}} \right) \times (1000/T_c) \text{gcm}^{-3}. \quad (5)$$

Using a linear interpolation of the Table 3 of Pollack et al. (1994) showing the sublimation temperature (T_{sub}) in terms of ρ_{disk} , we estimate $T_{sub} = 1417K$ at $R = R_{mag}$. We use $\dot{M} = 5 \times 10^{-9} M_{\odot} \text{yr}^{-1}$ and $T_c = 1000K$ as typical for the disk.

The temperature in the warp ($T_{mag} = T_c(R_{mag})$) is calculated using the model of an optically thick wall heated by the stellar radiation presented in D'Alessio et al. (2005) and used in Nagel et al. (2010) to calculate the emission of the wall heated by a binary stellar system. For the stellar parameters given in Table 1 and a typical dust composition and the grain size distribution proportional to the power-law $s^{-3.5}$ between a minimum grain size $s_{min} = 0.005\mu\text{m}$ (according to

the value used to characterize the interstellar medium (ISM), Mathis et al. 1977) and a maximum grain size $s_{max} = 1mm$ (assuming that in the disk the grains increase their size from $s_{max} = 0.25$ typical of the ISM), $T_{mag} = 1309K$. Because $T_{mag} \leq T_{sub}$ then the answer to the stated question is: the warp contains dust, such that the assumption of an optically thick structure is valid. Note that for V715 Per, the affirmative answer is important because this means that the disk at R_{mag} is the dust reservoir for the magnetospheric streams.

4.2. Is there dust inside the magnetosphere?

The disk material at R_{mag} is forced to move along the B-lines (because the magnetic pressure is equal to the ram pressure) filling the magnetosphere with a specific gas distribution. The density in this region allow us to calculate T_{sub} and with a comparison with the dust temperature T_{dust} we can check if there is dust in the magnetosphere as it is required to explain the light curve of V715 Per. In order to check if there is dust in the magnetosphere, we follow the next simple estimate. The use of ρ_{mag} from equation 2 is included in the full modeling. The gas density in this region ρ_{mag} depends on \dot{M} and the time it takes to arrive to the stellar surface starting its journey at R_{mag} . The mean of ρ_{mag} is calculated as

$$\langle \rho_{mag} \rangle = M_{gas,mag} / V_{mag}, \quad (6)$$

where $V_{mag} = \frac{4\pi}{3} R_{mag}^3$ is the volume of the magnetosphere and $M_{gas,mag}$ is the gaseous mass inside the magnetosphere, estimated with

$$M_{gas,mag} = \dot{M} \times t_{ff}, \quad (7)$$

where $t_{ff} = R_{mag} / v_{ff}$ with the free-fall velocity given by

$$v_{ff} = \sqrt{2GM_{\star}/R_{\star}} \sqrt{1 - R_{\star}/R_{mag}} \quad (8)$$

Doing the required substitution in the previous equations, we find that $\langle \rho_{mag} \rangle = 2.93(5.29) \times 10^{-15} g cm^{-3}$ and $T_{sub} = 1019(1038)K$ for $M_{\star} = 0.906(0.56)M_{\odot}$. The two values for T_{sub} correspond to the two values for M_{\star} (see Table 1). It is important to note that both values for T_{sub} are similar such that the uncertainty in M_{\star} is not relevant for the results presented here. Assuming a more realistic estimate for $\langle \rho_{mag} \rangle$, considering that the material is restricted inside an axisymmetric stream limited by magnetic field lines in the dipolar configuration ($r \propto \sin^2\theta$), we estimate that only 12% of the magnetospheric volume is covered with material. Because T_{sub} is not highly dependent on ρ , the new estimate ($T_{sub} = 1094(1106)K$) is close to the previous one. The estimate

of T_{sub} comes from a linear interpolation of Table 3 of Pollack et al. (1994). Assuming an optically thin environment with typical dust composition and grains size distribution (see Section 4.1), the estimated temperature in the magnetosphere is $T_{mag} \sim 1309\text{K}$ which is larger than T_{sub} . This temperature is at the outskirts of the magnetosphere. There is not dust in a region close to the magnetospheric spots, where the temperature is up to $\sim 7000\text{K}$. Starting at some minimum radius, there is a shell of evaporating dust up to R_{mag} . In order to find the gas temperature inside the magnetosphere, Hartmann et al. (1994) assume a volumetric heating rate $\propto R^{-3}$ coming from a flux of Alfvén waves during the gas accretion, which is cooled with a given radiative cooling rate. We conclude from this estimate that the grains will evaporate inside the magnetosphere.

In a study of the formation and evolution of chondrules inside a protoplanetary disk, Shu et al. (1996) estimate that the sublimation timescale, t_{sub} , is about a few hours when the grains are heated to above T_{sub} . Using the stellar parameters from Table 1, $t_{ff} = 6.79(7.56)\text{hours}$ ($M_{\star} = 0.906(0.56)M_{\odot}$). Thus it is reasonable to assume the existence of a dusty layer in the funnel flow because $t_{sub} \sim t_{ff}$.

For an estimate of the width of this layer, we included in this work the evaporating process as is described in Xu et al. (2018). The rate at which the grain size is reduced at the temperature T_{dust} is given by

$$\dot{s} = J(T_{dust})/\rho_{dust}, \quad (9)$$

where J is the net sublimation mass-loss flux and ρ_{dust} is the density of the dust grain, respectively. The expression for J is given by

$$J(T_{dust}) = \frac{\alpha_{subl}[P_{sat} - P_g]}{c_s \sqrt{(2\pi)}}, \quad (10)$$

and comes from the kinetic theory of gases. Here, α_{subl} is the evaporation coefficient, P_{sat} is the saturation pressure (where the condensation and sublimation are in equilibrium), $P_g = \rho_{mag} \times c_s^2$ is the gas pressure and finally c_s is the sound speed. Besides P_g , there are the gas ram pressure and the magnetic pressure which are in equilibrium. For the modeling, it is taken $\alpha_{subl} = 0.1$ and $\rho_{dust} = 3\text{g cm}^{-3}$ as typical values. The expression for P_{sat} is written as

$$P_{sat}(T_{dust}) = e^{-A/T_{dust}+B}, \quad (11)$$

with $A = 65000\text{K}$ and $B = 35$ for a generic refractory material (Xu et al. 2018). For the analysis presented in this work, A , B , ρ_{dust} and α_{subl} are fixed but the specific characteristics of the system that we do not know a priori will lead to changes in these values. The evaporation process occurs when $P_{sat} > P_g$ and condensation occurs when $P_{sat} < P_g$. For example at $T_{dust} = 1500\text{K}$ (typical

value for dust sublimation), the value for P_{sat} leads to condensation instead of sublimation. For $T_{dust} = 2000\text{K}$, P_{sat} increases in 5 orders of magnitude, such that the evaporation stage is reached. For $T_{dust} = 7000\text{K}$, P_{sat} increases 10 orders of magnitude more such that the dust only survives in a layer close to R_{mag} where T_{dust} is close to 1500K.

As mentioned in Section 4.1 the grains are distributed according to a power-law, in the Appendix A we show that during the evaporation process the power of the size distribution is conserved. Also in the Appendix A, we explain how the opacity at each point in a stationary stream is calculated which includes the fact that the evaporation decreases the dust abundance.

Because the power-law shape of the size distribution is conserved, the survival of dust can be analyzed with the survival of the grain in the magnetosphere with the largest size s_{max} using equation 9. We describe this process using a two steps algorithm. The steps are: 1) For each point in the magnetosphere we identify if it is located over a B-line that belongs to the stream limited by R_{in} and R_{out} (see Section 3.1). 2) Check if there is dust. The condition is: if $s_{max} \geq 0.25\mu\text{m}$ then there is dust at this point, see the Appendix A for details. The grains with sizes smaller than $s = 0.25\mu\text{m}$ will quickly disappear in the harsh environment the particle face from there on, following its trajectory towards the stellar surface. We use the ballistic velocity field of Hartmann et al. (1994), the shape of the B-line and equation 9 to describe the evaporation process along the trajectory. In this equation, we substitute ρ_{mag} from equation 2.

Repeating the two steps dust survival algorithm for every point in the region surrounding R_{mag} will lead to a dust distribution that depends on R , θ and ϕ . However, in order to estimate a typical radial width of the dusty layer, we apply the algorithm along different l os in order to sample the complete region and answer the question: How far in the stream the optically thin dust can survive? This depends on its temperature (T_{thin}) which for a given dust composition, grain size distribution and for a fixed stellar luminosity only depends on the distance to the star. For V715 Per at $R = 0.4R_{mag}$, $T_{thin} = 2221\text{K}$ which corresponds to $P_{sat} \gg P_g$. At this state, a grain of $s = 1\text{mm}$ sublimates in about 1hr which is a factor of 7 lower than t_{ff} , which means that at this location a grain rapidly disappear and dust closer to this radius is not present. At the outskirts of the stream at $R = R_{mag}$, $T_{thin} = 1479\text{K}$, $P_{sat} < P_g$ and the process is condensation instead of sublimation. This clearly means that the dust incorporating to the stream survive and steadily decrease in size until is completely evaporated as it moves in the stream towards the star. Between $R = 0.7$ and $R = 0.8R_{mag}$, $P_{sat} = P_g$ and the condensation turns into sublimation. This means that the dusty radial width is larger than $0.2R_{mag}$, thus, there is dust inside the magnetosphere that can shape the optical lightcurve. This estimate is done using a distribution of grains with $s_{max} = 1\text{mm}$. In Section 6, we show that according to the maximum grain size at the base of the stream, the radial width of the dusty layer varies.

Note that when the gas transit from the disk to the stream, probably there are a selection on the size of the grains that will do the journey because the first grains that incorporates to the stream are the ones located in the disk atmosphere where its size distribution is assumed to be consistent

with the dust in the ISM (this is because detailed disk models, such as in D’Alessio et al. (2006), show grain settling towards the midplane). Because we do not know the details of this process, a reasonable assumption is to consider that the grains size at the base of the stream are distributed according to a power-law with given s_{max} , which becomes the relevant free parameter to tune the modeling. In the Appendix A, details of the survival of dust as the material moves towards the star are shown.

5. Parameters for the modeling

5.1. Fixed parameters

From Grinin et al. (2018), we extract the stellar parameters (M_{\star} , R_{\star} , T_{\star}) noting that there are two values for M_{\star} : $0.56M_{\odot}$ (LeBlanc et al. 2011) and $0.906M_{\odot}$ (Kirk & Myers 2011). The distance to IC 348, where the source is located is 315pc. Using a mean of the estimates in Dahm (2008) we fix $\dot{M} = 5 \times 10^{-9}$. The light curve period is $P = 5.25$ days (Grinin et al. 2018), value that is very close to the rotational period of the star, $P_{rot} = 5.221$ days (Cohen et al. 2004). The inclination of the system is assumed as $i = 77$ deg, as the largest value expected such that the outside part of the disk is not blocking the stellar radiation (Nagel & Bouvier 2019).

Variations in the size distribution of the dust grains will change the opacity (κ) such that a consistent change on the stream dust to gas mass fraction (ζ_{stream}) will be required to explain the observations. In other words, there is a degeneracy between the last two variables. However, in the evaporation process that we include in the modeling, the grain size distribution is calculated at each point in the stream. The standard dust/gas mass fractions are fixed at typical values, $\zeta_{sil} = 0.004$ and $\zeta_{grap} = 0.0025$ for the silicate and the graphite components, such that $\zeta_{std} = \zeta_{sil} + \zeta_{grap} = 0.0065$. Using this, we fix κ . In the same process ζ_{stream} is calculated because surface material continuously evaporates from each grain, as the particles moves from the base of the stream towards the star. This means that the spatial distribution of dust including the grain size distribution (a power-law with a consistently calculated s_{max}) is taken into account when using the algorithm for dust survival (see Section 4.2).

5.2. Free parameters

According to the modeling, the dust responsible to shape the light curves is located in the magnetosphere. As ρ_{mag} is consistent with the observed \dot{M} then in order to explain the depth of the section of the light curve interpreted as the stellar eclipse with the magnetospheric streams, we focus on one free parameter, the maximum grain size at the base of the stream $s_{max,base}$.

As it is explained in the Appendix A the grain size distribution at the base of the stream is a power-law with an exponent -3.5 with a minimum grain size $s_{min} = 0.005\mu\text{m}$ and the maximum grain size $s_{max,base}$ is taken as the only free parameter. Its range is between $0.25\mu\text{m}$, the value associated to the interstellar medium (ISM) (Mathis et al. 1977) and 1mm, a value typical of the densest environment in a protoplanetary disk. Note that κ changes more than an order of magnitude

between the large grains distribution and the small grains distribution, thus, it can be tuned through $s_{max,base}$ to explain the amplitude of the lightcurve. Using κ , the gas density (ρ_g) and ζ_{stream} we can check on each los that the dust is optically thin. Including the grain evaporation, the system state moves towards an optically thin scenario, the basic requirement to explain the observations.

6. Modeling

The three states of the light curve are: 1) a 5.25d periodic signal of $\Delta mag \sim 0.1$, 2) a 5.25d periodic signal that decreases in amplitude ($\Delta mag < 0.1$) and 3) very deep Algol-like minima reaching amplitudes up to $\Delta mag = 1$ in a timescale of days. At any time of the observations there is a periodic signal with evolving amplitude, the Algol-like minima is superposed to the periodic signal. However, in the latter case, the dominant behavior is the one with the larger amplitude signal. As mentioned by Grinin et al. (2018), all states are interpreted by stellar extinction, such that the changes on the amount of dust surrounding the object should explain the observed variability. The state 1 is the one we explain in detail in Section 6.1, where we use dust distributed along the B-lines consistent with the value used for \dot{M} such that we name it, the low- \dot{M} state.

The state 2 is interpreted by Grinin et al. (2018) based on the assumption that a larger \dot{M} reduces R_{mag} such that the blocking structure decreases its area resulting in a decrease of Δmag . The variability of \dot{M} is suggested by the measurements of $EW(H_\alpha)$ at different times by Herbig (1998), Luhman et al. (1998) and Dahm (2008). The first two were taken outside the epoch of enhanced activity represented in the observations by the last one; thus it is sampled both regimes. Our interpretation differs from the previously stated: a larger \dot{M} (leading to a more powerful accretion shock) means a decrease on the amount of dust occulting the star because the stellar heating increases. A state with a larger \dot{M} is expected in Classical T-Tauri stars caused by their intrinsic variability. The Algol-like minima identifying the state 3 is simply an UX Ori-like event (stochastic fluctuations of the circumstellar extinction) where material continuously accumulating is explosively released to the star. The duration of the Algol-like minima is about a week such that the delivery of an unusual amount of gas (and dust) occurs continuously during (1-2) stellar rotations.

6.1. The low- \dot{M} state: fiducial models

The value for \dot{M} for V715 Per is estimated by Dahm (2008) using different optical and infrared lines. We name the models presented in this section, the fiducial models because we are just including the stellar heating as the only source of heating.

All the interpretation of the results is based on two competing mechanisms, the first one is that when in all the cells of the system $P_{sat} < P_g$ the system is on the non-evaporating stage, on the other hand when $P_{sat} > P_g$ the system is in the evaporating stage. Note that an increment of $s_{max,base}$ decrease T_{dust} and with this P_{sat} decreases, eventually making the system prone to condensation instead of sublimation, resulting in a large optical depth. Decreasing $s_{max,base}$ from its maximum value, the system changes from the non-evaporating stage to the evaporating stage. The latter stage

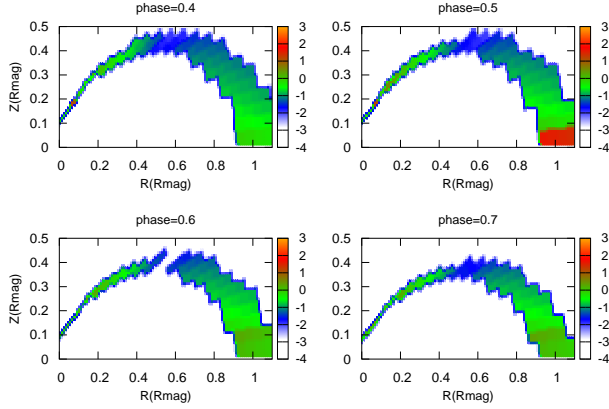


Fig. 1. The color map representing the density for different phases. This is part of the data used to find the light curves in Figure 3. Here, we show the model with $s_{max,base} = 1\text{mm}$.

is mixed with the other mechanism: an increment of the grain size decreases κ , resulting in a decrement of the optical depth (τ). Thus, in the evaporating stage, the evaporation in itself reduces the opacity because an amount of dust disappears but on the other hand the evaporation reduces the grain size and the opacity increases.

The light curves depend on the gas density distribution and the opacity of the dust located in the gaseous structures. Because of this, we present color maps of ρ_g and κ for an azimuthal cut at different phases showing the case with $s_{max,base} = 1\text{mm}$ in Figure 1 and 2. In Figure 1 is clear that the gas follows a stream along the magnetic lines in the dipolar configuration. Note that at different phases, the shape of the stream is different and the modulation by B_{pol} (see equation 2) stands out in the plot corresponding to $phase = 0.5$. In Figure 2, the low values of κ are associated to the large value for $s_{max,base}$. A small amount of evaporation is present at the tip of the stream.

The spatial distribution of dust (characterized by ζ_{stream} and s_{max}) is given using the evaporation algorithm (see details in Appendix A) such that the aim is to find $s_{max,base}$ consistent with $\Delta mag = 0.1$. The parameters used in the evaporation model implies that the dust can survive close to the star as can be seen in Figure 2.

For $s_{max,base} = 1\text{mm}$, $\Delta mag \sim 0.00724$, more than an order of magnitude lower than the value extracted from the observed light curves. For $s_{max,base} = 1\mu\text{m}$, $\Delta mag \sim 0.00917$, also less than expected. Note that these two models, while representing two extreme cases, produce similar small values for Δmag . This can be explained because for $s_{max,base} = 1\mu\text{m}$, ζ_{stream} decrease due to strong evaporation and for $s_{max,base} = 1\text{mm}$, is not important the evaporation but the opacity of large grains is small. This lead us to argue that there is a value of $s_{max,base}$ in between the previous values able to explain the observed Δmag . As shown in the modeled light curves presented in Figure 3, either $s_{max,base} = 10$ or $100\mu\text{m}$ are able to fit the requirement. In order to follow the trend in the light curves in Figure 3, we present the models for $s_{max,base} = 1, 10, 100\mu\text{m}$, and 1mm . The trend shown in Figure 3 is not monotonous, namely Δmag does not either increase or decrease when $s_{max,base}$ increase. We discuss the various modeled light curves in the following.

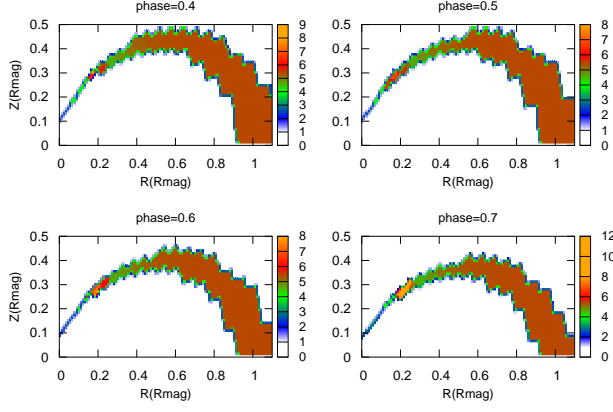


Fig. 2. The color map representing the opacity for different phases. This is part of the data used to find the light curves in Figure 3. Here, we show the model with $s_{max,base} = 1\text{mm}$.

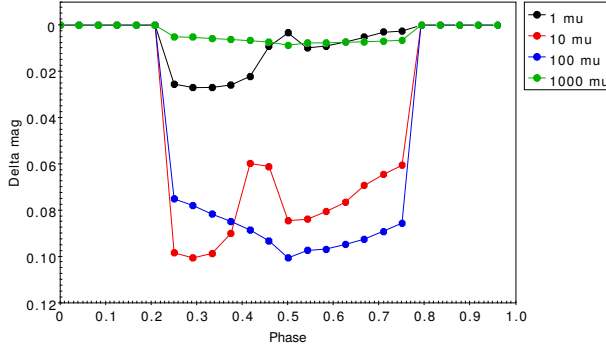


Fig. 3. The light curve for V715 Per consistent with $\dot{M} = 5 \times 10^{-9} M_{\odot} \text{yr}^{-1}$; $s_{max,base} = 1\mu\text{m}$ (black line), $s_{max,base} = 10\mu\text{m}$ (red line), $s_{max,base} = 100\mu\text{m}$ (blue line), $s_{max,base} = 1\text{mm}$ (green line).

The shape of the light curves for $s_{max,base} = 1000\mu\text{m}$ (model A) and $100\mu\text{m}$ (model B) are similar. The model B has larger Δmag than model A which means that $\tau_{100} > \tau_{1000}$. Because the mean grain size $\langle s \rangle$ is smaller in model B, the opacity κ_{100} is larger (τ_{100} is larger) compared to the value in model A, such that this effect dominates over the decrement of κ_{100} due to the evaporation process.

The shape of the light curves corresponding to $s_{max,base} = 100\mu\text{m}$ (model B) and $10\mu\text{m}$ (model C) mainly differ because the maximum in Δmag shift from the $phase = 0.5$ to $phase = 0.3$. Model B is in the non-evaporating stage and Model C is in the evaporating stage because $P_{sat} \gg P_g$. The behavior of Model B is completely determined by non-evaporation but in the model C, the evaporation reduces ζ_{stream} which compensates the increment of κ due to the decrement of $\langle s \rangle$, resulting in $\Delta mag_{100} \sim \Delta mag_{10}$.

The shape of the light curves for $s_{max,base} = 10\mu\text{m}$ (model C) and $1\mu\text{m}$ (model D) are similar. However, $\Delta mag_1 \ll \Delta mag_{10}$, which means that the strong evaporation increasing from model C to model D leads to a dominant ζ_{stream} decrement over the κ increment associated to a decrement in $\langle s \rangle$.

The light curves of models B and C are different (see Figure 3). The main difference is that the maximum of Δmag changes from $phase = 0.5$ (the azimuthal configuration where the maximum in density is located) in the model B to $phase = 0.3$ in model C. In order to explain how the shape

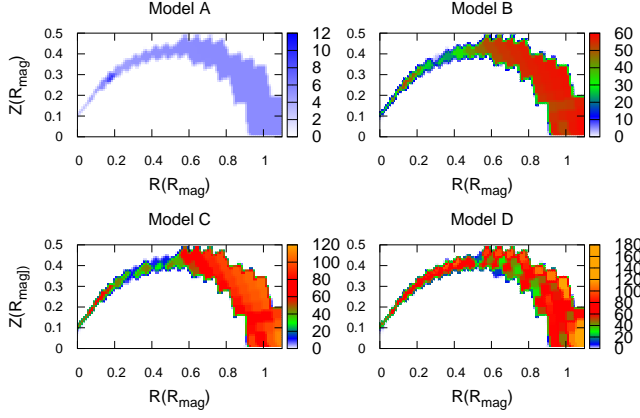


Fig. 4. The color map representing the opacity for the $phase = 0.3$. This is part of the data used to find the light curves in Figure 3. Here, we show the model A ($s_{max,base} = 1\text{mm}$, upper left plot), the model B ($s_{max,base} = 100\mu\text{m}$, upper right plot), the model C ($s_{max,base} = 10\mu\text{m}$, lower left plot), and the model D ($s_{max,base} = 1\mu\text{m}$, lower right plot).

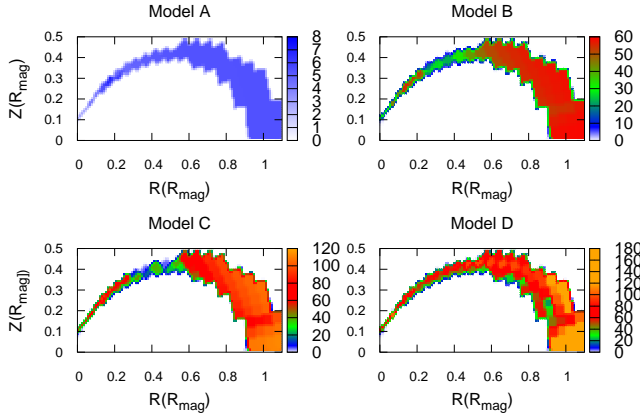


Fig. 5. The color map representing the opacity for the $phase = 0.5$. This is part of the data used to find the light curves in Figure 3. Here, we show the model A ($s_{max,base} = 1\text{mm}$, upper left plot), the model B ($s_{max,base} = 100\mu\text{m}$, upper right plot), the model C ($s_{max,base} = 10\mu\text{m}$, lower left plot), and the model D ($s_{max,base} = 1\mu\text{m}$, lower right plot).

of the light curves changes for different $s_{max,base}$, we present color maps for these two phases. The Figures 4 and 5 show κ color maps for different values of $s_{max,base}$ at $phase = 0.3$ and $phase = 0.5$, respectively. Note that in the model C, $\langle s \rangle$ decreases slower in a denser region because $\dot{s} \propto P_{sat} - P_g$, but at the same time τ decreases faster due to the amount of material evaporated. Besides $s_{max,base}$ decreases from model B to C, increasing κ . The result is that in model C at $phase = 0.5$ (largest density), the evaporation dominates over the other mechanisms increasing τ and at $phase = 0.3$, the increment of κ due to a smaller $s_{max,base}$ dominates over evaporation in a lower density region. This result in a shift of Δmag maximum between models B and C.

Note that, in the framework of this model, any way the dust is distributed, the only way to explain $\Delta mag = 0.1$ is with an optically thin scenario; a direct estimate of the required mean optical depth is $\langle \tau \rangle = 0.092$, which is consistent with the best-model presented.

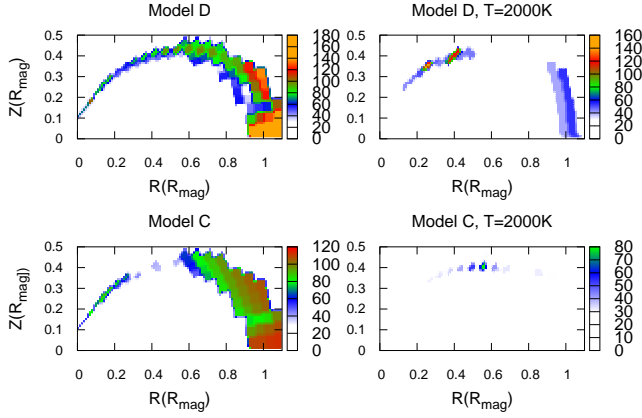


Fig. 6. The color map representing the opacity for the $phase = 0.5$. Here, we show the fiducial models: $s_{max,base} = 1\mu\text{m}$ (upper left plot), and $s_{max,base} = 10\mu\text{m}$ (lower left plot) complemented with the high temperature models: $s_{max,base} = 1\mu\text{m}, T_{dust} = 2000\text{K}$ (upper right plot), and $s_{max,base} = 10\mu\text{m}, T_{dust} = 2000\text{K}$ (lower right plot).

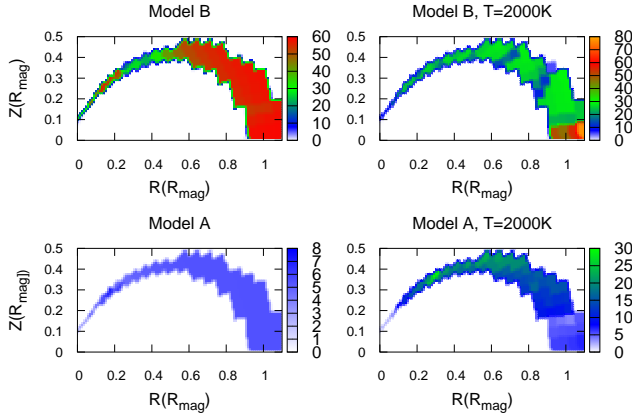


Fig. 7. The color map representing the opacity for the $phase = 0.5$. Here, we show the fiducial models: $s_{max,base} = 100\mu\text{m}$ (upper left plot), and $s_{max,base} = 1\text{mm}$ (lower left plot) complemented with the high temperature models: $s_{max,base} = 100\mu\text{m}, T_{dust} = 2000\text{K}$ (upper right plot), and $s_{max,base} = 1\text{mm}, T_{dust} = 2000\text{K}$ (lower right plot).

6.2. The low- \dot{M} state: higher temperature models

We name the models presented in this section, the high temperature models because we assume that the temperature can increase due to heating caused by the deposition of heat by Alfvén waves as mentioned in Hartmann et al. (1994). As explained in Section 4.2, the dust cannot survive at the high temperatures (up to $\sim 7000\text{K}$) present in most of the region limited by R_{mag} .

In order to analyze the effect of increasing the temperature, we show the opacity distribution for the cases $s_{max,base} = 1, 10, 100\mu\text{m}$ and 1mm when fixing T_{dust} to 2000K . The color maps are shown in Figures 6 and 7.

For all the models it is clearly seen that there is more evaporation than in the fiducial models. In Figure 7, we can see that the high temperature model with $s_{max,base} = 1\text{mm}$ shows an increase of the opacity compared with the fiducial model. In other words, P_{sat} increases such that $P_{sat} > P_g$, in this way reaching the evaporation stage. At this stage, the grain size decreases and the opacity increases. Because of the high inclination, the dust occulting the star is located close to R_{mag} where the opacity is the lowest, leading to a low-amplitude light curve which is not able to explain the

observed light curve. For the other models, the opacity decreases, such that these models are not able to explain the observed light curve. Our conclusion is that the survival dust is restricted to a thin layer where the precise width depends on a detailed modeling of the stream heating by Alfvén waves.

Note that the high temperature model with $s_{max,base} = 1\text{mm}$ in Figure 7 clearly shows that as the material moves towards the star, the opacity increases due to the decrease of s_{max} but finally there is an opacity decrease because the amount of material evaporated dominates over the decrement of s_{max} .

7. Conclusions

The main conclusions of the analysis and modeling of the dipper light curve of V715 Per are the following:

1) The dust can survive at R_{mag} where the disk is truncated for reasonable parameters for the density of the optically thick disk.

2) Assuming that the gas is distributed following the stellar B-lines and using the values for the observed \dot{M} , and a standard dust to gas ratio without evaporation, the dust in the magnetosphere is optically thick ($\langle \tau \rangle = 2.76$). However, in order to explain the observations we include evaporation, such that the required value $\langle \tau \rangle = \frac{2.3}{2.5} \times \Delta mag = \frac{2.3}{2.5} \times 0.1 = 0.092$ in the optically thin regime is consistent with the best model.

3) The low gas density and the radial range of the magnetosphere results that in most of it $T_{dust} > T_{sub}$, such that the dust cannot survive. Yet, the dust is able to survive in a shell with an outer radius given by R_{mag} , because the timescales for evaporation (t_{sub}) and free-fall towards the stellar surface (t_{ff}) are similar.

4) We find a model using as a free parameter, the largest size of the grains at the base of the magnetospheric stream, $s_{max,base}$. We find that the models with $s_{max,base} = 10, 100\mu\text{m}$ are able to explain the observed amplitude of the optical light curve (Δmag). The grains move towards the star and evaporate, changing their size and shaping the light curve.

5) The analysis of the models presented in Section 6.1 suggests that two competing mechanisms are simultaneously responsible for the shape of the the light curves. The first one is the evaporation that reduces the dust density leading to a decrement of the dip amplitude. However, during this process, the mean size of the grain decreases and the dip amplitude increases because the grain opacity increases. As $s_{max,base}$ changes, the contribution of both mechanisms also changes, thus the depth and shape of the light curves vary accordingly.

6) In the modeling, we do not include a model of deposition of heat by Alfvén waves in the stream as suggested by Hartmann et al. (1994), which would considerably increase the temperature inside the magnetosphere. At such a high temperature ($\sim 7000\text{K}$) the grains evaporate almost instantly, thus restricting the dust to a thin layer very close to R_{mag} . In any case, due to the high in-

clination of the system, almost all the blocking structure is close to R_{mag} , a fact that can be checked in any of the color maps where the shape of the stream can be seen.

7) Because the values for M_* (the main parameter to calculate t_{ff}) and \dot{M} (the main parameter to calculate R_{mag}) for V715 Per are typical of many other systems showing this behavior in their light curves, this mechanism can be invoked to explain the light curves where the flux shows color changes associated to circumstellar extinction, which indicates the occulting dust is optically thin.

Acknowledgements. This project has received funding from the European Research Council (ERC) under the European Union's Horizon 2020 research and innovation program (grant agreement No 742095 ; SPIDI : Star-Planets-Inner Disk-Interactions; <http://www.spidi-eu.org>). E.N. appreciate the support at the Institut de Planétologie & d'Astrophysique de Grenoble (IPAG) by Observatoire des Sciences de l'Univers de Grenoble/Université Grenoble Alpes (OSUG/UGA) while in a sabbatical stay where part of this work was done.

References

- Alencar, S.H.P., Teixeira, P.S., Guimaraes, M.M., et al. 2010, A&A, 519, id.A88
- Baraffe, I., Chabrier, G., Allard, F., & Hauschildt, P.H. 1998, A&A, 337, 403
- Barsunova, O.Yu., Grinin, V.P., & Sergeev, S.G. 2013, Astrophysics, 56, 395
- Barsunova, O.Yu., Grinin, V.P., Sergeev, S.G., Semenov, A.O., & Shugarov, S.Yu. 2013, Astrophysics, 58, 193
- Barsunova, O.Yu., Grinin, V.P., Arharov, A.A., et al. 2016, Astrophysics, 59, 147
- Bouvier, J., Chelli, A., Allain, S., et al. 1999, A&A, 349, 619
- Cody, A.M., Stauffer, J., Baglin, A., et al. 2014, AJ, 147, id.82
- Cohen, R.E., Herbst, W., & Williams, E.C. 2004, AJ, 127, 1602
- Dahm, S.E. 2008, AJ, 136, 521
- D'Alessio, P., Hartmann, L., Calvet, N., et al. 2005, ApJ, 621, 461
- D'Alessio, P., Calvet, N., Hartmann, L., Franco-Hernández, R., & Servin, H. 2006, ApJ, 638, 314
- D'Antona, F., & Mazzitelli, I. 1997, Mem.Soc.Astron.Ital., 68, 807
- Dodin, A.V., & Lamzin, S.A. 2012, Astronomy Letters, 38, 649
- Flaherty, K.M., Muzerolle, J., Rieke, G., et al. 2013, AJ, 145, 66
- Fonseca, N.N.J., Alencar, S.H.P., Bouvier, J., Favata, F., & Flaccomio, E. 2014, A&A, 567, A39
- Gregory, S.G., Jardine, M., Gray, C.G., & Donati, J.F. 2010, Reports on Progress in Physics, 73, 6901
- Grinin, V.P., Barsunova, O.Yu., Sergeev, S.G., Sotnikova, N.Ya., & Demidova, T.V. 2006, Astronomy Letters, 32, 827
- Grinin, V.P., Stempels, H.C., Gahm, G.F., et al. 2008, A&A, 489, 1233
- Grinin, V.P., Barsunova, O.Yu., Sergeev, S.G., et al. 2018, Astronomy Reports, 62, 677
- Hartmann, L., Hewett, R., & Calvet, N. 1994, ApJ, 426, 669
- Herbig, G.H. 1998, ApJ, 497, 736
- Kirk, H. & Myers, P.C. 2011, ApJ, 727, 64
- Konigl, A. 1991, ApJ, 370, L39
- LeBlanc, T.S., Covey, K.R., & Stassun, K.G. 2011, AJ, 142, 55
- Luhman, K.L., Rieke, G.H., Lada, C.J., & Lada, E.A. 1998, AJ, 508, 347
- Luhman, K.L., Stauffer, J.R., Muench, A.A., et al. 2003, ApJ, 593, 1093
- Lynden-Bell, D. & Pringle, J.E. 1974, MNRAS, 168, 603
- Mathis, J.S., Rumpl, W., & Nordsieck, K.H. 1977, ApJ, 217, 425
- McGinnis, P.T., Alencar, S.H.P., Guimaraes, M.M., et al. 2015, A&A, 577, A11
- Morales-Calderón, M., Stauffer, J.R., Hillenbrand, L.A., et al. 2011, ApJ, 733, id.50
- Nagel, E., D'Alessio, P., Calvet, N., et al. 2010, ApJ, 708, 38
- Nagel, E., & Bouvier, J. 2019, A&A, 625, A45
- Pollack, J.B., Hollenbach, D., Beckwith, S., et al. 1994, ApJ, 421, 615
- Romanova, M.M., Ustyugova, G.V., Koldova, A.V., et al. 2013, MNRAS, 430, 699

- Ruiz-Rodríguez, D., Cieza, L.A., Williams, J.P., et al. 2018, *MNRAS*, 478, 3674
- Sicilia-Aguilar, A., Manara, C.F., de Boer, J., et al. 2020, *A&A*, 633, A37
- Shu, F.H., Shang, H. & Lee, T. 1996, *Science*, 271, 1545
- Stauffer, J., Cody, A.M., McGinnis, P., et al. 2015, *AJ*, 149, 130
- Stauffer, J., Cody, A.M., Rebull, L., et al. 2016, *AJ*, 151, 60
- Xu, S., Rappaport, S., van Lieshout, R., et al. 2018, *MNRAS*, 474, 4795

Appendix A: Abundance, opacity and grain size distribution of the dust in the evaporating magnetospheric stream.

As the grains in the magnetospheric stream moves towards the star, P_{sat} surpass P_{gas} and the dust starts to evaporate. This process is not instantaneous, the grain decreases its size at a rate given by \dot{s} as it is described in Section 4.2. During this process, all the grains decrease in size, in the following we will show that the power-law grain size distribution is conserved.

The number of grains within the size range $[s, s+ds]$ are: $Cs^{-3.5}ds$, with C a normalization coefficient. The number of grains is conserved after the span of time dt , if ds changes to $\dot{s}dt + ds$. The size distribution, $f(s, t)$, satisfies the equation

$$f(s, t) \times (\dot{s}dt + ds) = Cs^{-3.5}ds, \quad (\text{A.1})$$

which can be written as

$$(Cs^{-3.5} - f(s, t))ds - f(s, t)\dot{s}dt = dg(s, t) = 0. \quad (\text{A.2})$$

Here g is a constant. From the total differential we can identify the terms $\frac{\partial g}{\partial s}$ and $\frac{\partial g}{\partial t}$ and using the fact that $\frac{\partial^2 g}{\partial s \partial t} = \frac{\partial^2 g}{\partial t \partial s}$, we found that

$$-\frac{\partial f}{\partial t} = \dot{s} \frac{\partial f}{\partial s}. \quad (\text{A.3})$$

The previous equation can be solved using the initial condition $f(s, t = 0) = Cs^{-3.5}$ such that $f(s, t) = Cs'^{-3.5}$, where $s' = s - \dot{s}t$ is the size of the grain after time t . Note that the power-law is conserved with the same exponent.

In a stationary configuration, each location of the stream has assigned a value for s_{max} . In the ISM and in the disk, the typical size distributions are characterized with a $s_{min} = 0.005\mu\text{m}$, for simplicity we keep this value here. For the estimate of s_{max} we use \dot{s} which requires the radial velocity given in Hartmann et al. (1994) calculated for ballistic infall from rest at R_{mag} used to calculate the density, such that s_{max} decreases as the dust moves closer to the star.

The dust opacity at each point is calculated as a time dependent process starting with the opacity of the large grains distribution ($s_{max} = s_{max,base}$) associated with the dust in the disk finally arriving to the case where $s_{max} \geq 0.25\mu\text{m}$, $s_{max} = 0.25\mu\text{m}$ is the value associated to a small grains distribution typical of the ISM, the lowest value considered here. A grain with $s_{max} < 0.25\mu\text{m}$ completely evaporates in a span of time small compared to the time it takes to arrive to this point. Thus, we assume that there is dust in a streamline if $s_{max} \geq 0.25\mu\text{m}$.

The opacity associated to the dust distributed with $0.25\mu m < s_{max} < 1mm$ is calculated interpolating between the opacity of the large grains and the small grains distribution of the standard abundance, $\zeta_{std} = 0.0065$.

We correct the opacity including the fact that the dust abundance decreases as each grain decreases in radius in the gradual evaporation of its superficial mass. This process should be done starting from the base of the stream.

The correction factor is calculated using the total initial dust mass (M_{init}) in a volume ΔV and the mass evaporated M_{evap} in a time span Δt .

From the initial dust abundance ζ_{init} , $M_{init} = \zeta_{init}\rho_g\Delta V$, where ρ_g is the gas density. On the other hand, we can write

$$M_{init} = \int_{s_{min}}^{s_{max}} C s^{-3.5} \rho_{dust} \frac{4\pi}{3} s^3 ds. \quad (\text{A.4})$$

Equating both expressions

$$C = \frac{3\zeta_{init}\rho_g\Delta V}{8\pi\rho_{dust}[s_{max}^{0.5} - s_{min}^{0.5}]}. \quad (\text{A.5})$$

After the integration time Δt , the evaporated dust mass is

$$M_{evap} = \int_{s_{min}}^{s_{max}} C s^{-3.5} \rho_{dust} \frac{4\pi}{3} (s^3 - (s - \dot{s}\Delta t)^3) ds. \quad (\text{A.6})$$

The corrected dust abundance ζ is calculated using

$$\zeta\rho_g\Delta V = M_{init} - M_{evap}, \quad (\text{A.7})$$

and doing all the straightforward integrations.

Now, for the next integration time $s_{max} = s_{max} - \dot{s}\Delta t$ and $\zeta_{init} = \zeta$ and this algorithm is repeated until the requested stream point is reached.